Int. J. Electrochem. Sci., 15 **(2020)** 5133 – 5143, doi: 10.20964/2020.06.21

International Journal of
ELECTROCHEMICAL
SCIENCE
www.electrochemsci.org

Electrophoretic Deposition of Superhydrophobic Al/Fe_2O_3 Nanothermite with Long–Term Storage Stability

Haibing Zhang[1], *Haitao Wu*[1], *Peng Xu*[2], *Zidong Li*[1], *Wuyang Zhang*[1], *Huixian Huang*[1], *Qing Zhou*[1], *Xingui Yue*[1], *Jiankang Bao*[1], *Xueming Li*[2,*]

[1] State Grid Chongqing Electric Power Company, Chongqing 400015, China
[2] School of Chemistry and Chemical Engineering, Chongqing University, Chongqing 400044, China
[*]E–mail: xml301@cqu.edu.cn

Received: 8 January 2020 / *Accepted:* 17 February 2020 / *Published:* 10 May 2020

In this study, a superhydrophobic Al/Fe_2O_3 nanothermite with long–term storage stability was prepared by electrophoretic deposition of nano–Al particles and nano–Fe_2O_3 microboxes on Ti substrate and subsequent modification process. The composition and morphology of Al/Fe_2O_3 nanothermite were systematically characterised through X–ray diffraction and scanning electron microscope. In addition, the water contact angle measurements and the immersion test demonstrated the excellent superhydrophobic properties of the as–prepared Al/Fe_2O_3 nanothermite. 10 days after underwater immersion, the heat release of the superhydrophobic Al/Fe_2O_3 nanothermite remained 982.7 J/g, which was higher than 514.6 J/g of the sample without superhydrophobic treatment. This work provides a beneficial sight for enhancing the long–term storage stability of nanothermite in practical application.

Keywords: Nanothermite; Heat release; Superhydrophobic; Stability; Al/Fe_2O_3

1. INTRODUCTION

Thermite, which consists of fuel (Al) and oxidizer (Fe_2O_3, CuO, MoO_3, NiO, Bi_2O_3, MnO_2, etc.) [1-13], has attracted extensive attention and been widely studied because of its promising application in the field of propulsion [14], ignition [15], gas generation [16] and other fields. One attractive feature of thermite is high combustion temperature and excellent heat release. It can provide a large amount of heat output in a short time when thermite is ignited. However, poor exothermic performance greatly inhibits their large–scale applications. According to previous reports, nano–sized thermite has higher heat output and lower onset ignition temperature than conventional micron–sized thermite due to shorter mass

diffusion distance [17]. Unfortunately, the nano–Al has a large specific surface area [18], which is easy to react with water vapor or oxygen in the air atmosphere during long–term storage and transportation, resulting in significant degradation of exothermic performance. Thus, it is urgent to design and fabricate controllable nanothermite with long–term storage stability.

Many recent efforts have been devoted to the development of nanothermite with long–term storage stability [19, 20]. Zhou et al. [21] reported that a glancing angle deposition method can be used to make the CuO/Mg/fluorocarbon core/shell nanoenergetic array with good long–term storage stability. Yu et al. [22] synthesized a distinctive Co_3O_4/Al core/shell nanowires (NWs) by combining magnetron sputtering and fluoroalkylsilane coating modification. 24 h after underwater storage, the energy output is ~ 50%, which exhibits good storage stability. Yang et al. [23] obtained nano–Al/PVDF microsphere particles by electrospray deposition. The nano–Al/PVDF microsphere particles displayed excellent intense combustion reaction. PVDF could effectively inhibit oxidation processes of micro/nano–Al particles, thus improving their stability during storage. Unfortunately, the complexity and inconveniences of these methods limit their large–scale practical application.

Superhydrophobic treatment is another promising strategy to enhance the oxidation resistance of nano–Al due to the unique advantages of low cost and convenience for large–scale preparation. Recently, superhydrophobic treatment has been widely used in oil–water separation [24-28], construction [29-32], medical applications [33, 34], corrosion prevention [35-39] and other fields. Nanothermite with superhydrophobic properties could inhibit water vapor adsorption on its surface, reduce the oxidation rate of nano–Al, and enhance the stability of nanothermite during storage. Ke et al. [17] reported a superhydrophobic Al/Fe_2O_3 nanothermite film based on electrophoretic deposition and surface modification technologies which displayed high superhydrophobicity and excellent long–time storage stability. In addition, other researchers [40-42] have applied a similar strategy of surface superhydrophobic modification to synthesize nanothermite with high oxidation resistance. Superhydrophobic surface modification is expected to realize the long–term storage performance of the nanothermite. The thermite composed of Al and Fe_2O_3 is a conventional energetic composite with a theoretical heat output of 3.98 kJ/g (equation 1). At present, there are few explorations about superhydrophobic Al/Fe_2O_3 nanothermite with high exothermic and long–term storage properties.

$$2Al+Fe_2O_3 \rightarrow Al_2O_3+2Fe \quad Q=3.98\ kJ/g \quad (1)$$

In this work, we have successfully fabricated the superhydrophobic Al/Fe_2O_3 nanothermite by facile electrophoretic deposited and subsequent surface modification process (in Scheme 1). The phase composition and morphology of Al/Fe_2O_3 nanothermite were characterized by X–ray diffraction and scanning electron microscope, respectively. In addition, exothermic performance and wettability of the samples were systematically studied by DSC and water contact angle measurements, respectively. The results provide useful references for the practical application of superhydrophobic Al/Fe_2O_3 nanothermite.

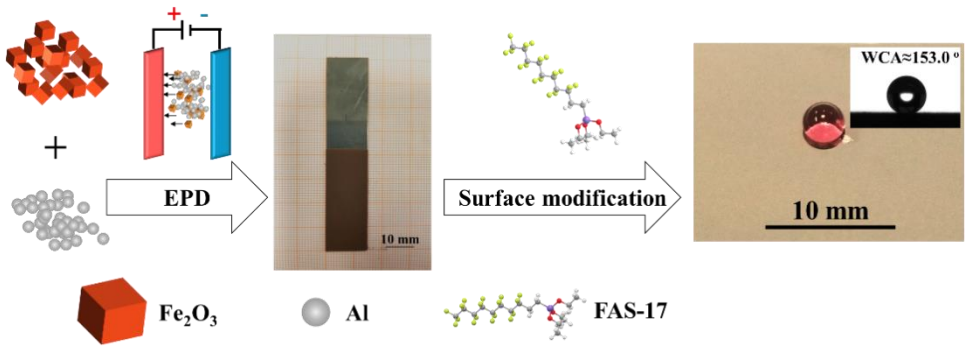

Scheme 1. Schematic illustrations for fabricated Fe_2O_3@Al nanothermite.

2. EXPERIMENTAL

2.1 Reagents and materials

Al nanoparticles (50 nm, 99%), Potassium ferrocyanide ($K_4Fe(CN)_6 \cdot 3H_2O$) and Poly(vinylpyrrolidone) (PVP, K–30, MW~40,000) were acquired from Aladdin (Shanghai, China). Poly(4–vinylpyridine) (P4VP, MW~60,000) was obtained from Aldrich (Shanghai, China). Hydrochloric acid, absolute ethanol, fuchsine and isopropanol were purchased from Chengdu Chron Chemicals Co,.Ltd. (Sichuan, China). All reagents were analytically pure and used directly without any further purification.

2.2 Preparation of Fe_2O_3 microboxes

The Prussian blue (PB) microboxes were synthesized according to the previous report [43-45]. Typically, PVP (7.60 g) and $K_4Fe(CN)_6 \cdot 3H_2O$ (0.22 g) were successively dissolved in 100 ml of 0.1 M hydrochloric acid. After keeping magnetic stirring for 30 min, the mixture was transferred to an oven for 24 h at 80 ^oC. The obtained blue products were then filtered and washed several times with absolute ethanol and distilled water. Subsequently, the products were dried in a vacuum oven for 2 h at 60 ^oC. Finally, Fe_2O_3 microboxes were prepared by annealing PB precursor in a furnace at 350 ^oC for 6 h with a temperate ramp of 5 ^oC min^{-1}.

2.3 Preparation of Al/Fe_2O_3 nanothermites by electrophoretic deposition

In this study, isopropanol was used as the solvent, and Al/Fe_2O_3 nanothermite was prepared on the Ti substrate by electrophoresis deposition (EPD). The Fe_2O_3 microboxes synthesized in this study had good dispersibility in isopropanol. No additional surfactant was used in the electrophoretic solution to promote dispersion of the nano–Al and Fe_2O_3 microboxes. Prior to the electrophoretic deposition process, the polished Ti electrodes with 1.5×8 cm^2 were ultrasonically cleaned using deionized water and absolute ethanol. The electrophoretic deposition parameters were set to a field strength of 200 V and

a deposition time of 10 min. The total mass of the particles in the 100 ml suspension was strictly controlled to 0.10 g. The obtained Al/Fe_2O_3 nanothermites was then dried in a vacuum oven at 80 °C for 2 h.

2.4 Characterization

Phase composition and micrograph were characterized by a scanning electron microscopy (SEM, JSM–7800F, JEOL, Japan) with an energy dispersive spectroscopy (EDS) and X–ray diffraction (XRD). The Al/Fe_2O_3 powders before and after the modification of FAS–17 were also characterized by FT–IR spectroscopy (FT–IR, Nicolet iS50, Thermo Scientific, USA) over the range 4000 to 400 cm^{-1}. Differential scanning calorimetry (DSC, STA449F3, NETZSCH, Germany) experiments were measured from 20 ^oC to1000 ^oC in Ar at a scanning speed of 20 ^oC/min. Water contact angle measurements were conducted on a contact angle meter (CA, Dataphysics OCA20, Germany). The wettability of superhydrophobic samples was evaluated directly by immersing the samples in aqueous solution of fuchsine.

3. RESULTS AND DISCUSSION

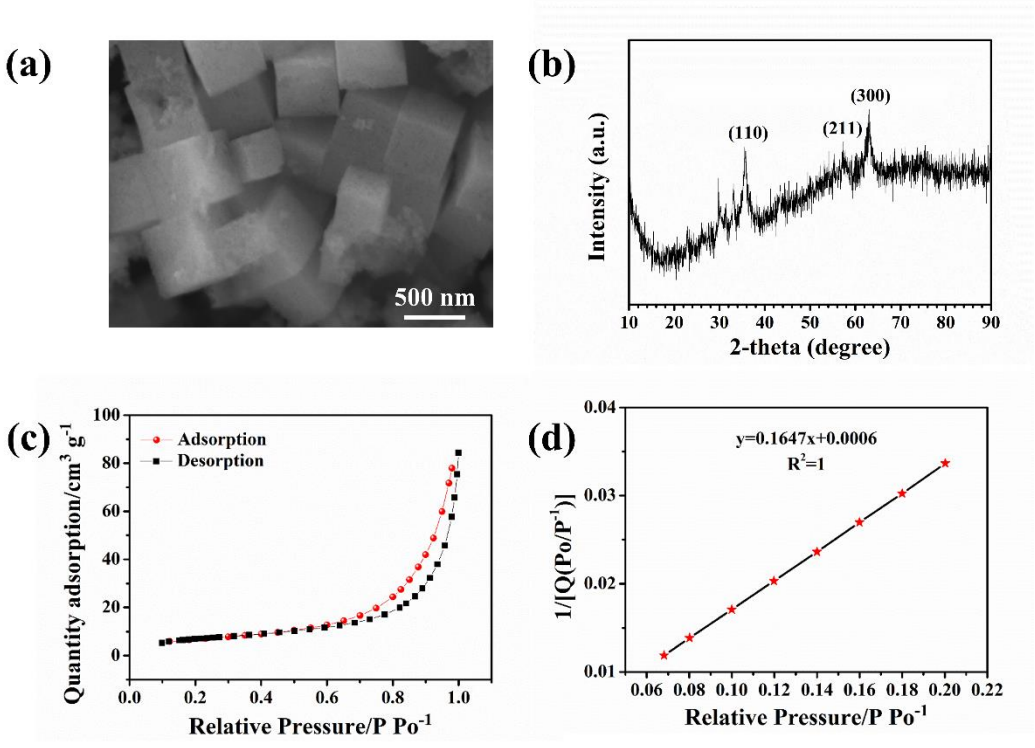

Figure 1. (a) SEM; (b) XRD; (c) N_2 adsorption–desorption isotherms and (d) their respective BET surface area linear fitting plots for Fe_2O_3.

As presented in Fig. 1 (a), the as–prepared Fe_2O_3 microbox was uniform with a regular size of 300 nm. The decomposition of the PBs precursor changes the structure of the sample, which results in the transition of the structure conversion of the smooth cube to the porous microboxes. The XRD result of Fe_2O_3 which shows cubic phase of Fe_2O_3 was obtained (Fig. 1 (b)). The microstructure of the oxidizer has an important influence on the heat output rate of the thermite. As shown in Fig. 1 (c–d), the N_2 adsorption–desorption isotherms were examined to confirm the internal structure and specific surface area of as–prepared Fe_2O_3 microboxes. The specific surface area of the Fe_2O_3 microboxes could be calculated by fitting a straight line. Typically, the specific surface area of the sample can be calculated as follows [46]:

$$S_g = \frac{4.36}{W} V_m \quad (1)$$

where S_g (m^2 g^{-1}) represents the specific surface area of the sample, V_m (mL) is the monolayer saturated adsorption capacity, and W (g) represents the mass of Fe_2O_3 microvoxes. According to the linear equation y =0.1647x+0.0006, the specific surface area of Fe_2O_3 microboxes is 26.33 m^2/g, and the correlation coefficient (R^2) value of the linear equation is 1.

Fig. 2 (a) shows optical photographs of Fe_2O_3 films, Al films and Al/Fe_2O_3 films were prepared by EPD (from left to right). It can be clearly seen that these three films deposited on the Ti sheet are smooth, dense and uniform. The crystalline structure of Al/Fe_2O_3 film was characterized through XRD as shown in Fig. 2 (b). From the XRD patterns, all diffraction peaks can be assigned to the cubic phase of Al (JCPDS No. 04–0787) and cubic phase of Fe_2O_3 (JCPDS No. 39–1346). In addition, no other characteristic peak was observed, evidently confirming the high purity of the Al/Fe_2O_3. The reaction between Al and Fe_2O_3 was not carried out during the EPD process [47]. The result suggested that Al/Fe_2O_3 was successfully fabricated by a facile and effective electrophoretic deposition strategy. The Al/Fe_2O_3 was also characterized by FT–IR spectroscopy. As shown in Fig. 2 (c), the FT–IR spectrum of sample after the modification of FAS–17 exhibits representative distinctive peaks at 1237 cm^{-1}, 1206 cm^{-1} and 1148 cm^{-1} corresponding to C–F bending. In addition, characteristic peak of Si–O–Si was observed at 1069 cm^{-1} [48 -50]. The result means that Al/Fe_2O_3 film was successfully modified by FAS–17 after immersion in 1% (% v/v) FAS–17 ethanol solution of 10 min.

SEM and EDS were performed to further investigate the microstructure and element composition of the samples. In this work, porous Fe_2O_3 microboxes were successfully fabricated through a simple one–pot reaction and subsequent annealing (shown in Fig. 2 (d)). It is clearly seen that the synthesized Fe_2O_3 microboxes, with the diameter of ~350 nm, reveal rough surfaces and display nearly uniform cube–like structures.

As shown in Fig. 2 (e), the nano–Al particles with a diameter of ~ 100 nm used in this study present a uniform spherical shape. It is well observed in Fig. 2 (f–g) that Al and Fe_2O_3 in the samples prepared by EPD were evenly distributed without obvious agglomeration. EDS and elemental mapping showed that as–prepared Al/Fe_2O_3 EMs showed signals containing Al, Fe, O and F, which proved that these elements were evenly distributed and successfully modified by FAS–17.

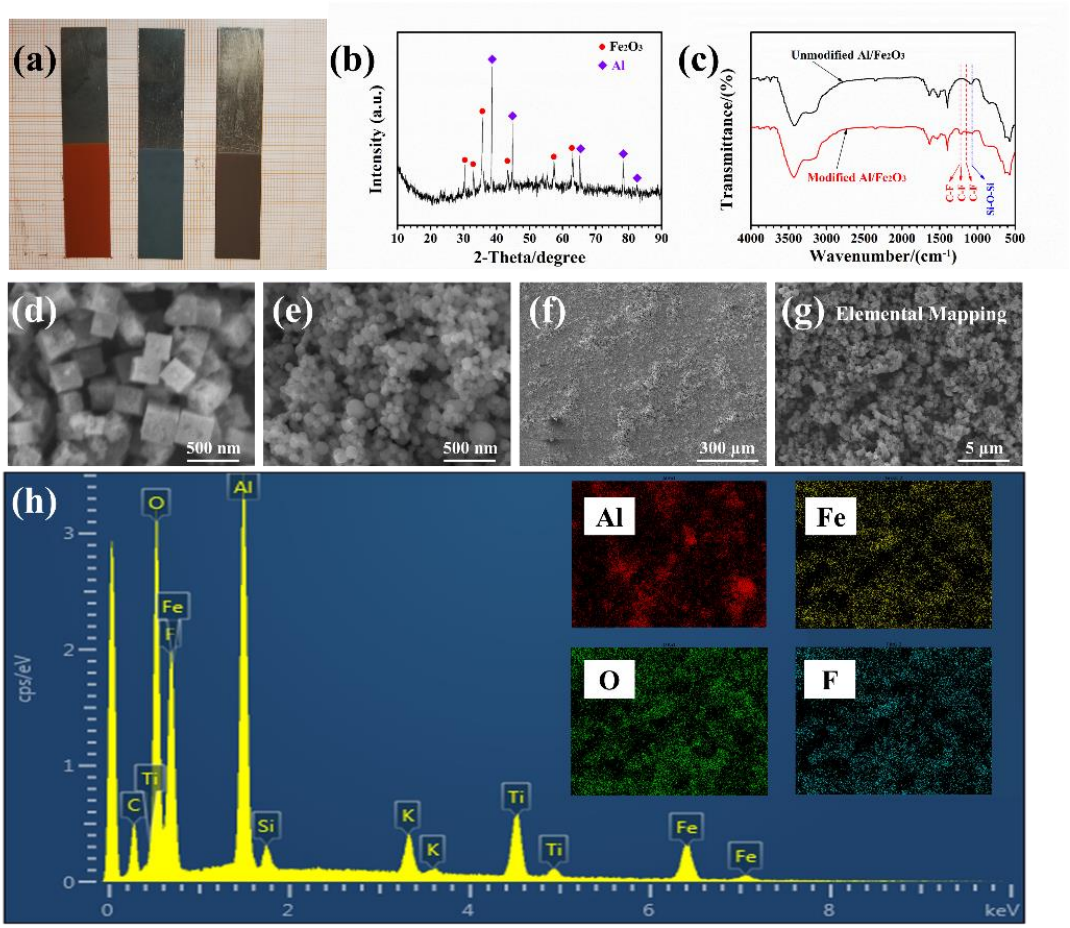

Figure 2. (a) The optical photographs of Fe_2O_3, Al and Al/Fe_2O_3 (from left to right). (b) XRD pattern of Al/Fe_2O_3. (c) FT–IR spectra of Al/Fe_2O_3 before and after surface modification. (d) SEM image of Fe_2O_3 microboxes. (e) SEM image of nano–Al particles. (f–g) SEM images of Al/Fe_2O_3. (h) EDS result and elemental mapping images of Al/Fe_2O_3.

To determine heat release performance, the exothermic reaction of Al/Fe_2O_3 nanothermite were studied by DSC. As can be seen in Fig. 3 (a), the onset reaction temperature of the self–assembled Al/Fe_2O_3 nanothermits was observed at 540 ^oC and a strong exothermic peak appeared at 592 ^oC. The endothermic peak that occurs at a temperature of 656.9 °C is attributed to the melting of the nano–Al. The heat release of the thermal reaction reaction is mainly derived from the solid–solid reaction between nano–Al and Fe_2O_3. The total reaction heat of the Al/Fe_2O_3 thermite reaction is up to 1504 J/g through the DSC thermal analysis software. The mass ratio of Al nanoparticles to Fe_2O_3 microboxes has an important effect on the heat release of the thermite reaction. Higher heat output can be obtained by precisely adjusting the mass of Al added in the self–assembly process.

The exothermic behavior of Al/Fe_2O_3 nanothermite with different equivalent ratios was further investigated, and the obtained data are shown in Fig. 3 (b). In Fig 3 (b), an increase in the equivalent ratio of nanoparticles in the suspension (from 0.5 to 1.5) resulted in a gradual increase in heat output from 1069 J/g to 1504 J/g. However, the increased equivalent ratio (from 1.5 to 2.5) did not continue to promote the exothermic performance of Al/Fe_2O_3 nanothermites. The Fe_2O_3 microbox cannot react with excessive nano–Al completely, thus the exothermic efficiency decreased. Therefore, we found that the

maximum heat release of the Al/Fe_2O_3 nanothermites prepared in this study at an equivalent ratio of 1.5 was 1504 J/g.

Many efforts have been directed toward the the thermal analysis of nanothermites. The exothermic reaction behavior of Al/Fe_2O_3 pellet nanothermites were determined by Zhou and his co–authors [51]. Their work shows that the exothermic peak of Al/ Fe_2O_3 nanothermite pellet is 545.8 ±2 ^oC, and the heat release value is 1409 ± 91 J/g. In contrast, the Al/Fe_2O_3 nanothermite prepared by EPD in this work exhibited excellent exothermic performance of the same grade. Beside, the EPD method, as a convenient method, can prepare films on conductive substrates of various shapes. Compared with the vapor deposition method, the electrophoretic deposition method can be applied to prepare thermite in non–vacuum environment and room temperature. These advantages enable the electrophoretic deposition to deposit thermites on chips for use in microelectromechanical systems (MEMS).

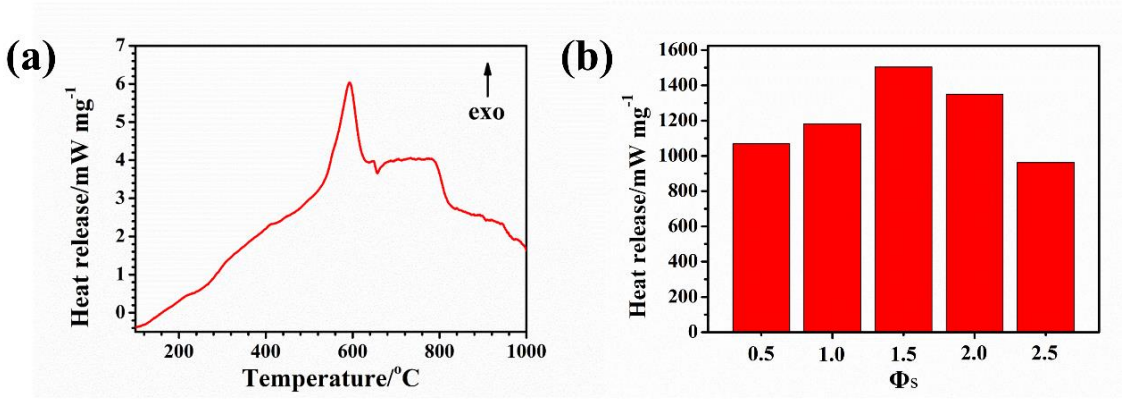

Figure 3. (a) The DSC curve of (a) Al/Fe_2O_3 nanothermite and (b) The heat release of Al/Fe_2O_3 nanothermite with different equivalent ratios of 10 min under field strength of 100 V.

The surface of Al/Fe_2O_3 was superhydrophobically treated by surface modification. As shown in Fig. 4 (a), there are many tiny pore structures in Al/Fe_2O_3 formed by EPD on the electrode of Ti sheet. The superhydrophobicity of the prepared samples is guaranteed by the micro/nano structure and the modification of low surface energy materials. When droplets contact with the surface of superhydrophobic Al/Fe_2O_3, the sample cannot be rapidly wetted. Therefore, the oxidation resistance of Al/Fe_2O_3 was improved, which enhanced its long–term storage stability further. The optical photo of superhydrophobic Al/Fe_2O_3 is shown in Fig. 4 (b). Clearly, droplets of red fuchsin are spherical on the surface of superhydrophobic Al/Fe_2O_3. And the small droplets can easily roll. The contact angle test results showed that the contact angle of the droplet on the superhydrophobic Al/Fe_2O_3 surface was about 153 ^{o} (inset in Fig. 4 (b)). The hydrophobic angle of the sample was significantly increased after superhydrophobic treatment (Fig. S1). In past work [40, 41], it was shown that the contact angle of the nanothermite treated by FAS–17 is more than 167 ^{o}. However, the contact angle of the Al/Fe_2O_3 nanothermite in this work is only 153 ^{o}, which is caused by the difference of the microstructure of the thermite particles.

The immersion test is widely used as a conventional verification method to visually evaluate the superhydrophobic properties of superhydrophobic films. In this work, immersion tests were carried out to evaluate the superhydrophobic properties of Al/Fe_2O_3 samples modified by FAS–17. A series of optical photographs of the immersion test are shown in Fig. 4 (c). The test results showed that silver–white air layer appeared on the surface of the superhydrophobic sample when it was immersed in the red solution. However, when the superhydrophobic sample was removed upward, there was no residual red liquid on the surface of the sample. The surface of the sample was dry without obvious peeling. These phenomena mean that the prepared samples have good superhydrophobic properties and can effectively inhibit water wetting. In practical applications, it is expected that the samples can inhibit the oxidation of nano–Al by water vapor in the environment.

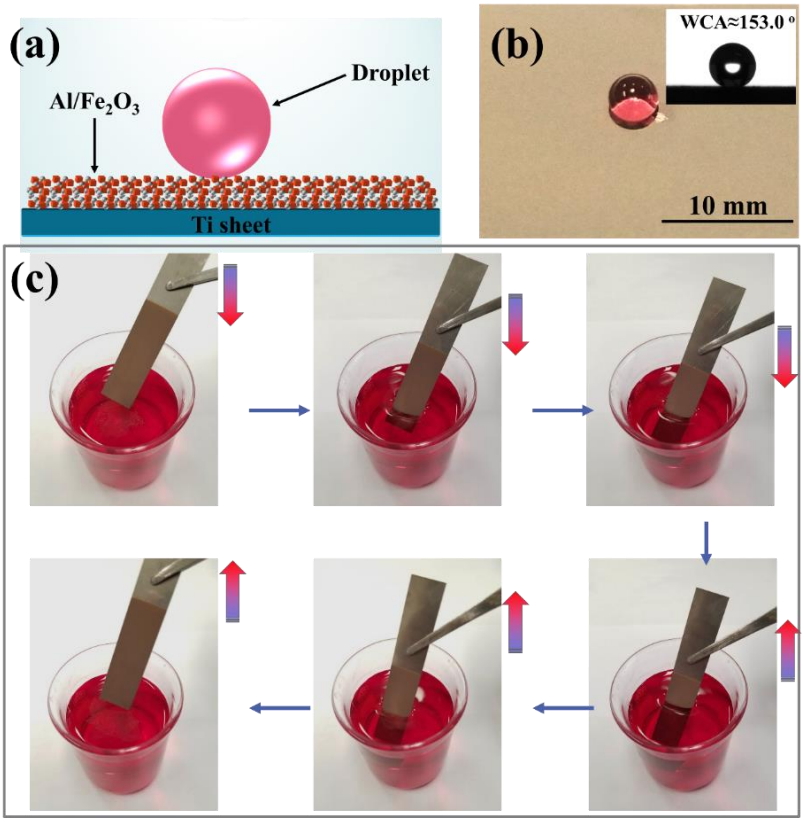

Figure 4. (a) Schematic diagram of superhydrophobic Al/Fe_2O_3. (b) optical photograph of superhydrophobic Al/Fe_2O_3; inset shows contact Angle test. (c) immersion test of samples.

To further investigate the effect of superhydrophobic treatment on long–term storage performance of Al/Fe_2O_3 nanothermites, DSC was used to evaluate the heat release of superhydrophobic treatment and untreated samples after 2, 4, 6, 8 and 10 days underwater accelerated aging test, respectively. Schematic diagram of underwater accelerated aging test is shown in Fig. 5. The prepared samples were immersed in 1.0 cm deep distilled water and the aging test was conducted at room temperature.

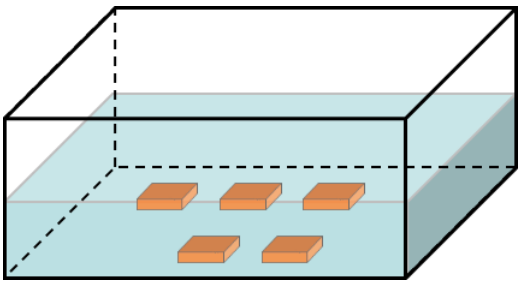

Figure 5. Schematic diagram of underwater accelerated aging test.

Fig. 6 shows the relationship between heat release and storage time of nanothermites treated with or without superhydrophobic treatment. The heat release of samples without superhydrophobic treatment was significantly lower than that of samples treated with superhydrophobic treatment. 10 days after submerged immersion, the unheated nano–Al particles gradually reacted with water and the active mass decreased, resulting in a decrease in the exotherm of the samples without superhydrophobic treatment from 1504 J/g to 514.6 J/g. Obviously, the heat release of the sample after the superhydrophobic treatment of nano–Al was only reduced by 982.7 J/g. This result indicates that the superhydrophobic treatment can effectively inhibit the reaction of nano–Al with water when being stored underwater. Further, the underwater aging test shows that the superhydrophobic treatment can enhance the long–term storage life of the nano–Al in air environment. Yu and her co–authors [22] investigated the exothermic performance of FAS–modified Co_3O_4/Al core/shell thermites stored underwater. The DSC results showed that the exothermic performance was retained about 50% after 2 days. In this study, the heat release of FAS–17 modified superhydrophobic Al/Fe_2O_3 nanothermite remained about 65% after 10 days of underwater storage. This result exhibies that the Al/Fe_2O_3 nanothermite prepared in this study has excellent long–term storage performance.

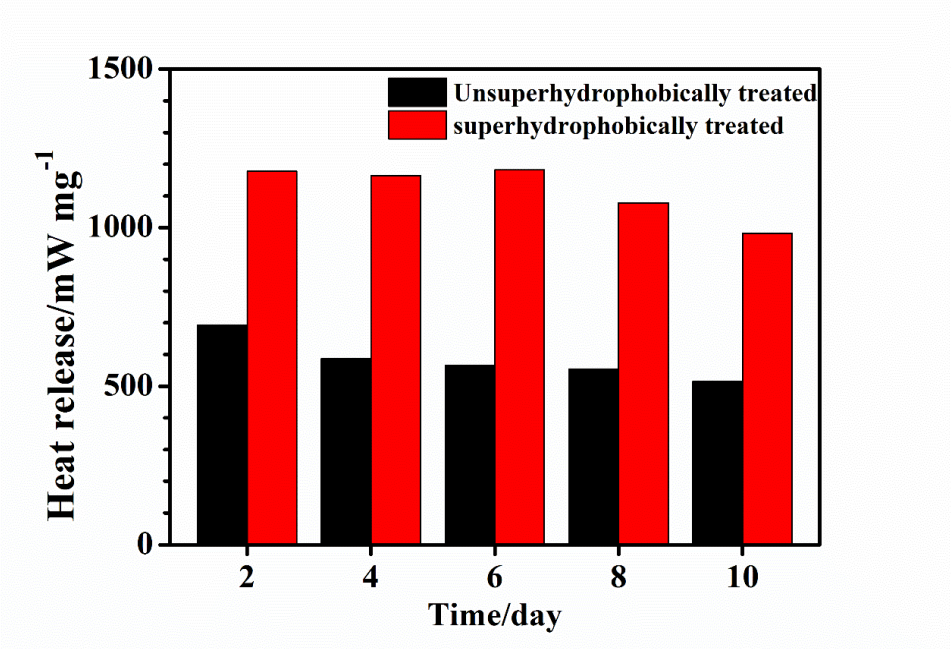

Figure 6. Relationship between heat release and differernt storage times of treated with and without superhydrophobic treatment nanothermites.

4. CONCLUSION

In summary, the novel superhydrophobic Al/Fe_2O_3 nanothermite was successfully synthesized by a simple electrophoretic deposition method and subsequent superhydrophobic modification process. In present study, the DSC test results show that the maximum heat output of Al/Fe_2O_3 nanothermite is 1504 J/g. After underwater immersion of 10 days, the heat release of the superhydrophobic Al/Fe_2O_3 nanothermite still reach 982.7 J/g. It is higher than the exotherm of the non–superhydrophobized modified sample of 514.6 J/g. The results show that the FAS–17 can insulate the water and keep the nano–Al stable. This work is of great significance to improve the long–term storage stability of nanothermite.

ACKNOWLEDGEMENTS
This research was funded by Chongqing Graduate Research and Innovation Project (No. CXB14220), Chongqing Municipal Training Program of Innovation and Entrepreneurship for Undergraduates (No. S201910611427) and National Natural Science Foundation of China (No. 61271059).

CONFLICT OF INTEREST
The authors declare that they have no conflict of interest.

References

1. C. Yu, W. Zhang, R. Shen, X. Xu, J. Cheng, J. Ye, Z. Qin, Y. Chao, *Materials & Design*, 110 (2016) 304-310.
2. C. Rossi, *Propellants Explosives Pyrotechnics*, 39 (2014) 323-327.
3. F. Severac, P. Alphonse, A. Esteve, A. Bancaud, C. Rossi, *Adv. Funct. Mater*., 22 (2012) 323-329.
4. J.Y. Ahn, J.H. Kim, J.M. Kim, D.W. Lee, J.K. Park, D. Lee, S.H. Kim, *Powder Technol*., 241 (2013) 67-73.
5. M.S. Shin, J.K. Kim, J.W. Kim, C.A.M. Moraes, H.S. Kim, K.K. Koo, *Journal of Industrial and Engineering Chemistry*, 18 (2012) 1768-1773.
6. D. Zhang, X. Li, B. Qin, C. Lai, X. Guo, *Mater. Lett*., 120 (2014) 224-227.
7. T.F. Zhang, Z. Wang, G.P. Li, Y.J. Luo, *J. Solid State Chem*., 230 (2015) 1-7.
8. F. Saceleanu, M. Idir, N. Chaumeix, J.Z. Wen, *Frontiers In Chemistry*, 6 (2018) 10.
9. Y. Zhu, X. Zhou, C. Wu, H. Cheng, Z. Lu, K. Zhang, *Sci Rep*, 7 (2017) 6678.
10. M.D. Grapes, R.V. Reeves, K. Fezzaa, T. Sun, J.M. Densmore, K.T. Sullivan, *Combust. Flame*, 201 (2019) 252-263.
11. K.J. Kim, M.H. Cho, J.H. Kim, S.H. Kim, *Combust. Flame*, 198 (2018) 169-175.
12. S. Deng, Y. Jiang, S. Huang, X. Shi, J. Zhao, X. Zheng, *Combust. Flame*, 195 (2018) 303-310.
13. Y. Yang, D. Xu, K. Zhang, *J. Mater. Sci*., 47 (2012) 1296-1305.
14. D. Xu, Y. Yang, H. Cheng, Y.Y. Li, K. Zhang, *Combust. Flame*, 159 (2012) 2202-2209.
15. Z.-Y. Zhu, B. Ma, C.-M. Tang, X.-L. Cheng, *Phys. Lett*. A, 380 (2016) 194-199.
16. C. Yu, W. Zhang, B. Hu, D. Ni, Z. Zheng, J. Liu, K. Ma, W. Ren, *Nanotechnology*, 29 (2018) 36LT02.
17. X. Ke, X. Zhou, G. Hao, L. Xiao, J. Liu, W. Jiang, *Appl. Surf. Sci.*, 407 (2017) 137-144.
18. J. Wang, Z. Qiao, Y. Yang, J. Shen, Z. Long, Z. Li, X. Cui, G. Yang, *Chemistry*, 22 (2016) 279-284.
19. X. Ke, X. Zhou, H. Gao, G. Hao, L. Xiao, T. Chen, J. Liu, W. Jiang, *Materials & Design*, 140 (2018) 179-187.
20. X. Ke, X. Zhou, G. Hao, L. Xiao, J. Liu, W. Jiang, *Appl. Surf. Sci*., 407 (2017) 137-144.
21. X. Zhou, D. Xu, G. Yang, Q. Zhang, J. Shen, J. Lu, K. Zhang, *ACS Appl. Mater. Interfaces*, 6

(2014) 10497-10505.
22. C.P. Yu, W.C. Zhang, Y. Gao, D.B. Ni, J.H. Ye, C.G. Zhu, K.F. Ma, *Chem. Eng. J.*, 338 (2018) 99-106.
23. H. Yang, C. Huang, H. Chen, *J. Therm. Anal. Calorim.*, 127 (2016) 2293-2299.
24. L. Liu, J.L. Lei, L.J. Li, R. Zhang, N.Y. Mi, H.R. Chen, D. Huang, N.B. Li, *Mater. Lett.*, 195 (2017) 66-70.
25. J. Chen, Y. Zhou, C. Zhou, X. Wen, S. Xu, J. Cheng, P. Pi, *Chem. Eng. J.*, 370 (2019) 1218-1227.
26. W. Hao, J. Xu, R. Li, X. Zhao, L. Qiu, W. Yang, *Chem. Eng. J.*, 368 (2019) 837-846.
27. M. Li, C. Bian, G. Yang, X. Qiang, *Chem. Eng. J.*, 368 (2019) 350-358.
28. K. Wang, X. Liu, Y. Tan, W. Zhang, S. Zhang, J. Li, *Chem. Eng. J.*, 371 (2019) 769-780.
29. H. Chen, Y. Jin, L. Lei, X. Ding, X. Li, Y. Wang, L. Sun, L. Shen, M. Yang, B. Wang, *Appl. Surf. Sci.*, 462 (2018) 149-154.
30. X. He, P. Cao, F. Tian, X. Bai, C. Yuan, *Surf. Coat. Technol.*, 357 (2019) 180-188.
31. Z. Wang, W. Yang, F. Sun, P. Zhang, Y. He, X. Wang, D. Luo, W. Ma, G.-C. Sergio, *Surf. Eng.*, 35 (2019) 418-425.
32. B. Zhang, W. Xu, Q. Zhu, Y. Li, B. Hou, *J. Colloid Interface Sci.*, 532 (2018) 201-209.
33. Z. Li, N. Ba Loc, Y.C. Cheng, J. Xue, G. MacLaren, C.H. Yap, *Journal Of Materials Chemistry* B, 6 (2018) 6225-6233.
34. R.M. Raj, V. Raj, *J. Coat. Technol. Res.*, 15 (2018) 51-64.
35. L. Liu, J.L. Lei, L.J. Li, J. Zhang, B. Shang, J.X. He, N.B. Li, F.S. Pan, *Advanced Materials Interfaces*, 5 (2018).
36. J.D. Brassard, D.K. Sarkar, J. Perron, A. Audibert-Hayet, D. Melot, *J. Colloid Interface Sci.*, 447 (2015) 240-247.
37. Y. Lin, Y. Shen, A. Liu, Y. Zhu, S. Liu, H. Jiang, *Materials & Design*, 103 (2016) 300-307.
38. N. Yang, J. Li, N. Bai, L. Xu, Q. Li, *Materials Science And Engineering B-Advanced Functional Solid-State Materials*, 209 (2016) 1-9.
39. R. Gao, Q. Liu, J. Wang, X. Zhang, W. Yang, J. Liu, L. Liu, *Chem. Eng. J.*, 241 (2014) 352-359.
40. X. Guo, X. Li, *Mater. Lett.*, 186 (2017) 357-360.
41. X. Guo, X. Li, C. Lai, X. Jiang, X. Li, Y. Shu, *Chem. Eng. J.*, 309 (2017) 240-248.
42. E. Nixon, M.L. Pantoya, G. Sivakumar, A. Vijayasai, T. Dallas, *Surf. Coat. Technol.*, 205 (2011) 5103-5108.
43. L. Zhang, H.B. Wu, X.W. Lou, *J. Am. Chem. Soc.*, 135 (2013) 10664-10672.
44. X. Li, Y. Liu, C.L. Zhang, T. Wen, L. Zhuang, X.X. Wang, G. Song, D.Y. Chen, Y.J. Ai, T. Hayat, X.K. Wang, *Chem. Eng. J.*, 336 (2018) 241-252.
45. Q. Teng, Y. Chen, X. Sun, Y. Wang, F. Li, L. Wang, J. Zhao, H. Wang, Y. Zhang, *J. Alloys Compd.*, 739 (2018) 425-430.
46. Y. Yin, X. Li, Y. Shu, X. Guo, H. Bao, W. Li, Y. Zhu, Y. Li, X. Huang, *Mater. Chem. Phys.*, 194 (2017) 182-187.
47. X. Guo, T. Liang, *Materials*, 12 (2019) 234.
48. H. Zhang, Y. Lu, X. Jin, B. Wang, T. Yang, H. Xu, H. Liu, C. Chao, *Mater. Res. Express*, 6 (2019) 105044.
49. C. Wang, C. Piao, X. Zhai, F. Hickman, J. Li, *Powder Technol.*, 200 (2010) 84–86.
50. Y. Fan, H. Liu, B. Xia, W. Zhu, K. Guo, J. Li, *Mater. Lett.*, 194 (2017) 81–85.
51. X. Zhou, Y. Zhu, X. Ke, K. Zhang, *J. Mater. Sci.*, 54 (2019) 4115–4123.